AD-A088 270 MASSACHUSETTS INST OF TECH LEXINGTON LINCOLN LAB F/G 17/5
ELECTRO-OPTICAL TESTS OF CCD IMAGERS AT THE GEODSS ETS.(U)
FEB 80 D F KOSTISHACK, C H GYLFPHE F19628-80-C-0002
UNCLASSIFIED TR-539 ESD-TR-79-326 NL

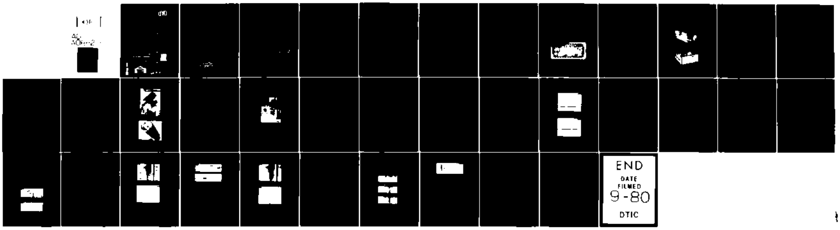

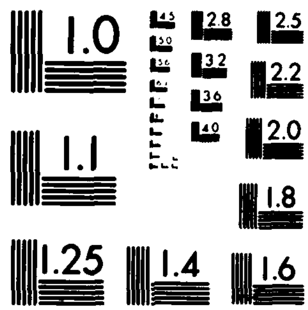

MICROCOPY RESOLUTION TEST CHART

NATIONAL BUREAU OF STANDARDS 1963 A

MASSACHUSETTS INSTITUTE OF TECHNOLOGY

LINCOLN LABORATORY

ELECTRO-OPTICAL TESTS OF CCD IMAGERS AT THE GEODSS ETS

D. F. KOSTISHACK

C. H. GYLFPHE, JR.

M. J. MacDONALD

N. G. S. PONG

Group 94

TECHNICAL REPORT 539

20 FEBRUARY 1980

LEXINGTON MASSACHUSETTS

ABSTRACT

As part of the GEODSS-CCD Technology Program, a series of three electro-optical tests of CCD imagers was conducted on the GEODSS Experimental Test System (ETS) at Socorro, New Mexico. The tests were preliminary to establish the basis for developing and testing an advanced CCD automatic detection system which would provide improved sensitivity and scan coverage rate for GEODSS applications. These preliminary tests resulted in the successful demonstration of STARE and image-motion-compensation (IMC) modes of operation, and provided a thorough evaluation and verification of present CCD system design models. Also, interesting electro-optical performance levels were demonstrated, compared with existing GEODSS system designs.

CONTENTS

ELECTRO-OPTICAL TESTS OF CCD IMAGERS AT THE GEODSS ETS

I. INTRODUCTION

In January and December 1978 and March 1979, a series of electro-optical tests was conducted on the GEODSS Experimental Test System (ETS) at Socorro, New Mexico on experimental CCD imagers as part of the GEODSS-CCD Technology Program at Lincoln Laboratory. The CCD imager chips tested were designed and fabricated through the joint technology program in the Space Surveillance Group and the Microelectronics Group. This report describes these tests and summarizes the data and results.

As part of the GEODSS Program in the Space Surveillance Group, several projects are directed at the development of technologies which could lead to an automatic search and detection system for satellite surveillance, with improvements in sensitivity and high scan coverage rate. This proposed system design is based on the unique features provided by charge-coupled-device (CCD) technologies for both optical imaging as well as video analog signal processing. The focal plain design for the proposed system incorporates a mosaic array of 25 to 30 CCD imager chips which are continuously scanned in the CCD image-motion-compensation (IMC) mode with multiple measurements provided by several imagers on-focal-plane in the scan direction for MTI processing. CCD imager and processing chips are being developed by the Microelectronics Group in support of this technology program design. A preliminary measurements program is presently under way to determine the electro-optical characteristics of these CCD imagers in laboratory measurements, as well as camera field tests using existing telescopes at the GEODSS ETS.

A. Site-Test Objectives

The overall objectives for the initial CCD camera site-tests were to evaluate the electro-optical, mechanical, and operational interfaces with the existing ETS sensors and to measure various aspects of CCD camera performance to allow a comparison with laboratory measurements and theoretical design predictions. Specifically, all interface requirements were to be satisfied and measurements taken on calibration stars and selected satellites to provide data on sensitivity, dynamic range, photo-responsivity, resolution, metric registration, acquisition capability for STARE and IMC, and effects of telescope dynamics for the IMC mode. The electro-optical experimental system and measurements were aimed at sensor characterization only. Although STARE and IMC modes were used and targets acquired, it was not intended or possible to conduct automatic searches with the existing imager electronic test system.

B. Results Summary

All site test objectives were achieved in this preliminary series of tests. Both STARE- and IMC-mode operation were successfully demonstrated for the single-chip CCD camera. Over the total of the periods of testing; more than 100 measurement observations were accomplished in approximately 6 nights of adequate seeing conditions, out of a total of 23 days at the ETS site.

The CCD electro-optical performance models were thoroughly evaluated and verified. Measurements agreed with the models for electro-optical responsivity and sensitivity to within a few tenths of a visual magnitude for both STARE and IMC modes.

Low-light-level calibration solar stars were visually detectable at magnitudes as low as 17.2 M_v for STARE mode and 15.9 M_v for IMC mode, with integration times of 0.9 and 0.25 sec, respectively. The observed signal-to-noise ratios were >6. These magnitudes agreed within a few tenths of a visual magnitude with the predicted electro-optical sensitivity which was modified from the ideal values to account for the size mismatch between the existing point-target image-seeing disc diameter and the CCD pixel size. In an automatic search system application, either the CCD pixel size and telescope focal-plane scale factor would have to be specified to yield an optimized match, or extensive real-time video signal processing would have to be implemented to maximize probability of detection.

The CCD imagers for these field-tests exhibited nominal quantum efficiencies of 20 to 30 percent, with camera electronic noise levels typically at 35 to 45 equivalent rms electrons. Successful techniques for focal-plane alignment, operating point adjustment, metric calibration, and object acquisition for IMC scans were developed.

II. EXPERIMENTAL SYSTEM

A. CCDs Tested

The series of tests was centered around developmental CCD imager chips designed to provide the requirements for the proposed CCD automatic search system. Table I lists the required and existing device parameters. As can be seen in the table, not all of the required chip capability had been achieved at the times of the tests. However, laboratory measurements of the existing parameters permitted useful design evaluation in these preliminary site-tests.

TABLE I

CCD REQUIREMENTS AND STATUS BY MARCH 1979

	100 × 400 CCD Characteristics	
	Goal	Status
Dark Current (nA/cm^2)	5	<5
Transfer Efficiency	0.99992	0.99998
Noise (electrons)	20	12
Quantum Efficiency (percent)	40	20 to 30
Dynamic Range	10^4	$\approx 2 \times 10^4$
Chip Alignment (mils)	±0.1	<±0.1
Defective Columns (percent)	<5	≈1.8

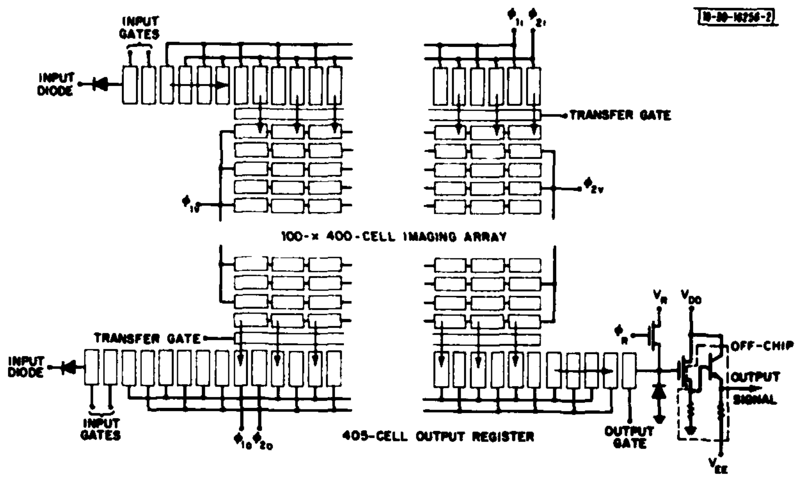

Fig. 1. Schematic of 100- × 400-pixel CCD image sensor.

A schematic diagram of the 100- × 400-pixel CCD is shown in Fig. 1. For operation as an imager only, the active 100 × 400 array, output register, and output circuits are used. The CCD imagers are two-phase, buried n-channel devices, using polysilicon gate electrodes, implanted column barriers, and input and output register blooming drains. The output floating-diffusion circuit includes a MOSFET amplifier followed by an off-chip bipolar transistor to drive the video circuit load.

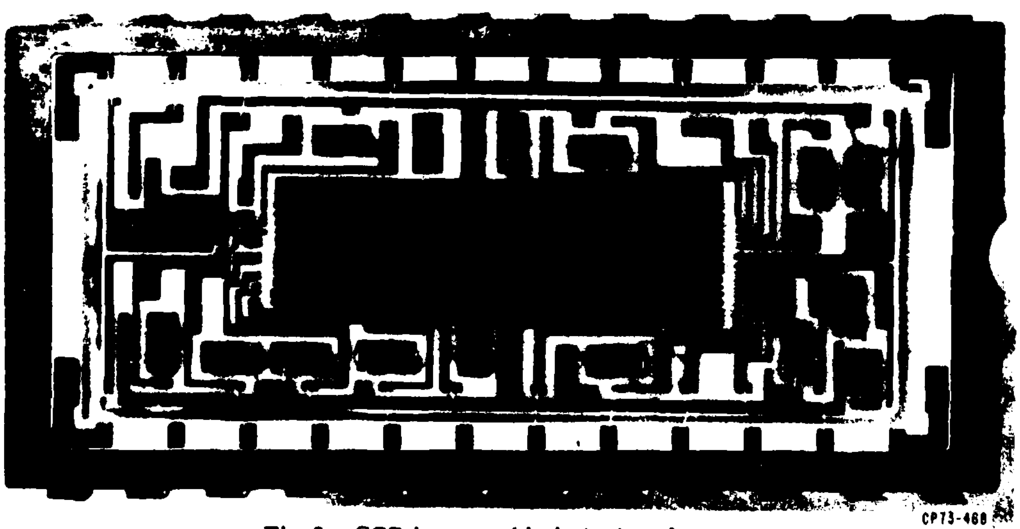

Fig. 2. CCD imager chip in test package.

The preliminary site-tests were conducted on single-chip focal planes. The CCD mounted in a single-chip package for testing is shown in Fig. 2. The imagers are front-illuminated through the polysilicon gates.

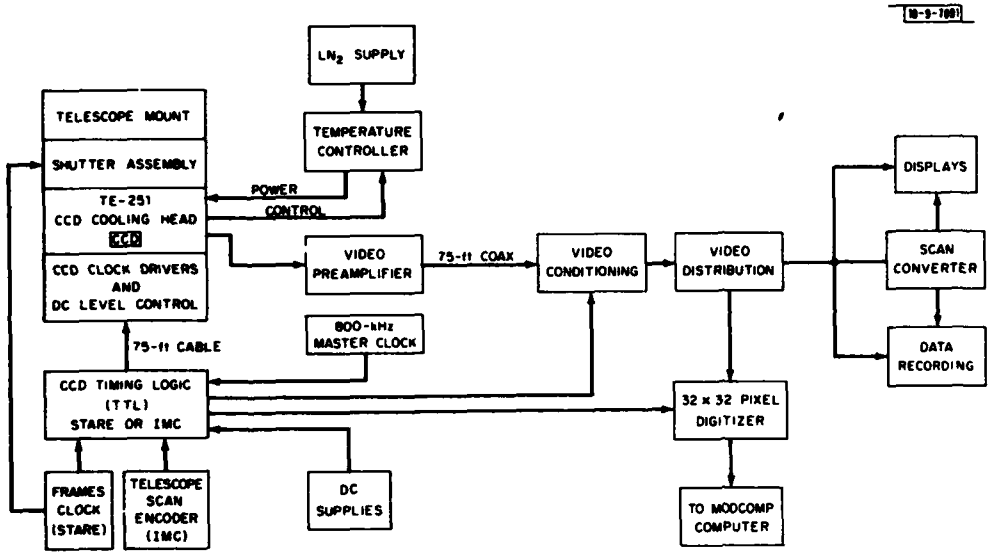

Fig. 3. CCD experimental camera system diagram.

B. CCD Camera Electronics

A block diagram of the experimental camera system for testing the individual imager chips is shown in Fig. 3. The CCD to be tested is mounted in a 24-pin socket in a refrigeration dewar which uses liquid nitrogen for coolant. A resistive "no-dew" heater is used to eliminate condensation and icing on the Plexiglas window. The high-power, high-speed drivers which supply the necessary clock levels to operate the CCD and DC level adjustments are located in the camera electronics assembly shown behind the chip dewar in Fig. 4. The timing logic which supplies the CCD drive clocks and display ramp generators, and the DC power supplies make up the controller assembly shown in Fig. 5.

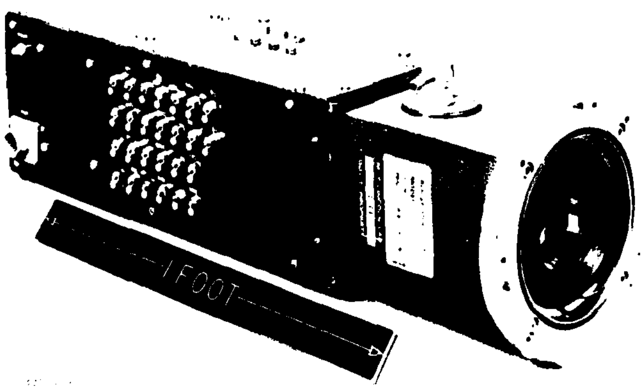

Fig. 4. Single-chip CCD camera.

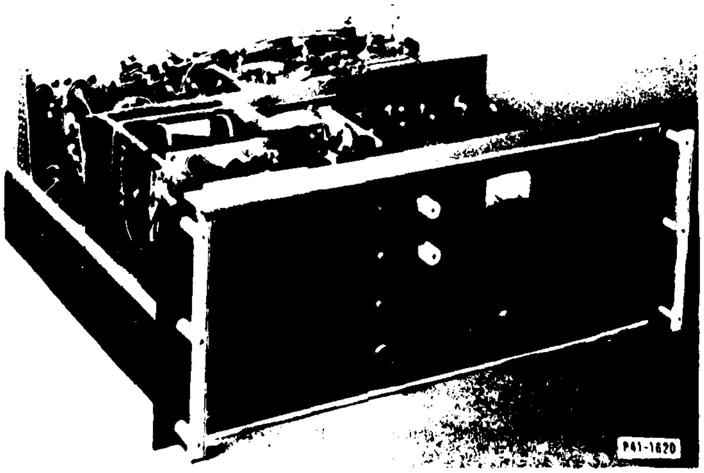

Fig. 5. CCD camera timing controller unit.

18-9-7092

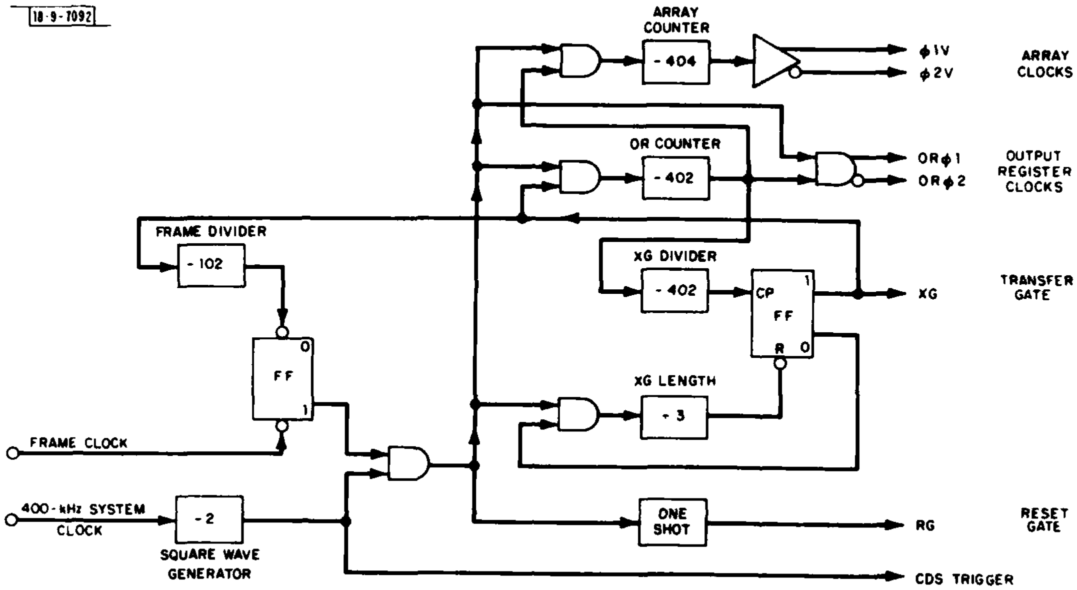

Fig. 6(a). CCD STARE-mode timing logic block diagram.

The timing logic is located on individual plug-in boards which are interchangeable, depending on the choice of either STARE or IMC mode of operation. A functional diagram of these logic circuits is shown in Figs. 6(a) and (b). Several options for frame timing such as lockup to optical shutters is possible with the STARE logic. The IMC logic permits lockup of the line transfer clocks of the CCD to pulses generated by the telescope axis encoders during IMC scans.

C. Video Electronics

For the objectives of these preliminary tests, the video from the CCD was first amplified by a low-noise video preamplifier-driver. Correlated double-sampling was used to remove various forms of clock leak-through and noise; and the imager video was fanned out to several offset buffer amplifier channels for displays and data recording. Figure 7 is a diagram of this analog video network.

D. Data Recording and Displays

Several types of displays and data recordings were used in the tests. The video clocked from the CCD imager is not in standard TV format. For example, in the STARE mode of operation a frame integration period selectable from 0.1 to 20 sec can be used. Following the integration period, the frame of video data is normally clocked out at a 400-kHz analog bit rate; that is, the 40,000 cells of the frame are read out in 0.1 sec. The video is displayed on a high-speed x-y-z monitor with synchronized ramps generated in the controller assembly logic. Either log or linear amplitude can be displayed.

The CCD video also was converted to standard TV composite video format which permitted display on TV monitors and recording on cassette video-tape recorders. For the IMC mode

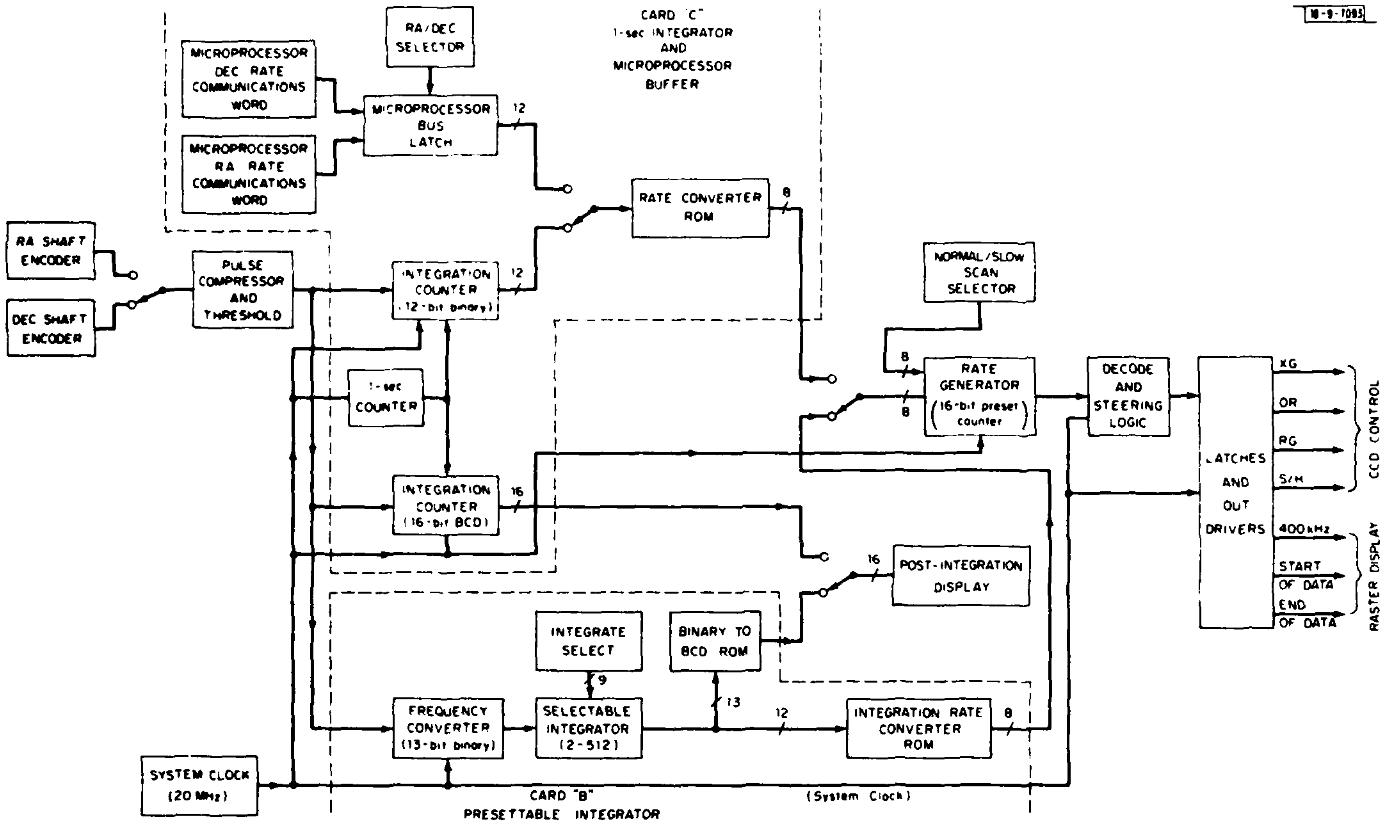

Fig. 6(b). IMC synchronizer control logic block diagram.

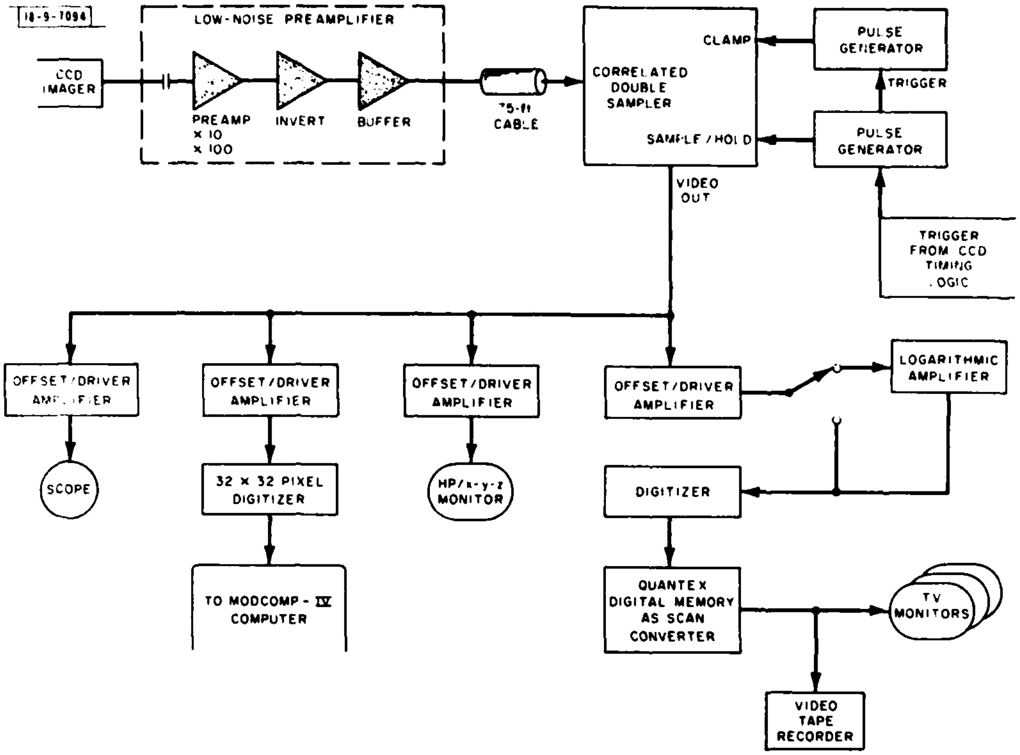

Fig. 7. Analog video network AND signal recording and display.

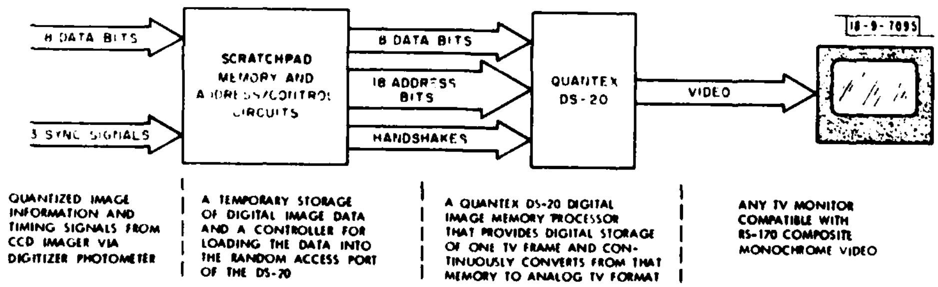

Fig. 8. Quantex/CCD scan converter.

tests, no image framing was provided by the CCD camera; therefore, scan conversion to TV was required for all IMC display and recording. For Site-Test II, two Princeton Electronic Product's CRT scan converters were multiplexed to store and convert alternate CCD fields-of-view. For Site-Test III, a Quantex DS-20 Digital Image Memory/Processor was used for scan conversion which provided a TV format covering four CCD fields-of-view. Figure 8 is a diagram of the Quantex scan-converter configuration. The expanded field-of-view was essential in enabling IMC scans through particular star and satellite targets of interest.

Amplitude measurements in STARE mode on calibrated point targets were taken with an oscilloscope displaying a selectable horizontal line of the video pulse shape of the target. An oscilloscope camera was used to record the video pulse displayed.

Initial tests were also conducted in STARE mode on a video digitizer-recording system which digitizes a selectable 32- × 32-pixel portion of the 100- × 400-pixel CCD array with a 12-bit dynamic range. The digitized point target amplitudes can be recorded by the ETS MODCOMP computers on magnetic tape for signal analysis and processing during and after observation periods.

Photographic cameras were also used to record observed star-satellite fields on the TV monitors.

E. Site-Test Configurations

The three CCD sensor site-tests involved the use of both large-aperture telescopes at the GEODSS ETS in both the Cassegrainian and prime focus configurations. Table II lists the optical parameters of each of the telescope options. In general, the Cassegrainian position for the focal plane provided greater resolution and ease in mechanically interfacing the CCD camera to the telescope. The prime focus position provided more desirable pixel size – seeing disc size match, enabling operation approaching designed performance and a somewhat larger field-of-view. Table II also indicates the specific telescope used for each of the three tests. Between the first

TABLE II

TYPICAL CHARACTERISTICS OF TELESCOPES AT THE GEODSS ETS FOR THE CCD ELECTRO-OPTICAL TESTS

	31-In. Cassegrain	31-In. Prime Focus	14-In. Folded Schmidt
f/Number	f/5	f/2.87	f/1.7
Field-of-View (deg)	1.16	2.0	7.0
Focal-Plane Scale Factor (mils/$\widehat{\text{sec}}$)	0.754	0.43	0.122
Effective Aperture (m^2)	0.20	0.29	0.039

Site-Test I: "B" system 31-in. Cassegrain
Site-Test II: "A" system 31-in. prime focus
Site-Test III: "B" system 31-in. prime focus

Fig. 9. "A" system telescopes at GEODSS ETS.

Fig. 10. CCD camera on 31-in. telescope at ETS in prime-focal position.

and second tests, the "A" telescope was modified by Boller & Chivens to permit locating cameras at the prime focus position with no interference between the telescope motion and dome motion. Therefore, for both Tests II and III the more desirable prime focus scale factor was used first on the "A" tower and later on the "B" tower systems.

For all tests, the wide-field 14-in. folded Schmidt telescopes at the ETS were used to assist in acquiring calibration stars and satellites of interest using the ETS Ebsicon camera systems.

The "A" system telescopes are shown in Fig. 9. In Fig. 10, the CCD camera is shown mounted on the "A" telescope used in Test II. As seen in the figure, the CCD camera structure was contained in a minimum-diameter profile in order to maintain maximum telescope aperture.

A simplified block diagram of the total site-test system is shown in Fig. 11. During the STARE mode testing periods, objects of interest were first located in the 14-in. telescope field-of-view. The telescopes were then slewed to move the targets into the limited field-of-view of the CCD imager which was outlined on the 14-in. monitor. Finally, the telescope operator would locate the target within the CCD field-of-view manually while observing the console TV display of the actual CCD imager video. For targets too dim to be observed by the 14-in. telescopes, the CCD camera was used directly to acquire the targets within known local star fields.

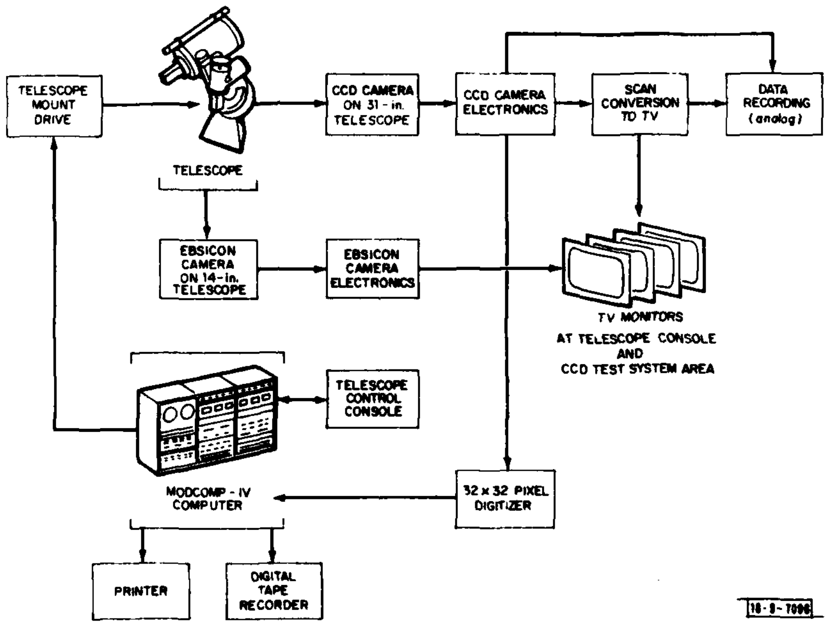

Fig. 11. CCD site-test system block diagram.

For the IMC mode testing, only positive declination scans were used to minimize camera realignment problems. Each measurement required that the object of interest be located first with the 14-in. telescope. The telescopes were then moved to position the target directly above the marked CCD field-of-view. The telescopes were then offset in negative declination several degrees before scan initialization. This large offset permitted the positive declination scan rate to stabilize before the target appeared in and scanned through the CCD field-of-view. Before the declination scan was enabled by calling up a computer-stored fixed rate, the right-ascension telescope mount drive was locked out so that only sidereal drive remained in RA. Once the scan was initiated and the object of interest was viewed on the 480- × 384-pixel scan-converted CCD video, a push button was operated which disabled rewriting of the memory contents of the video scan converter. This permitted recording of the target field-of-view with photos of monitor displays and video-tape recorders.

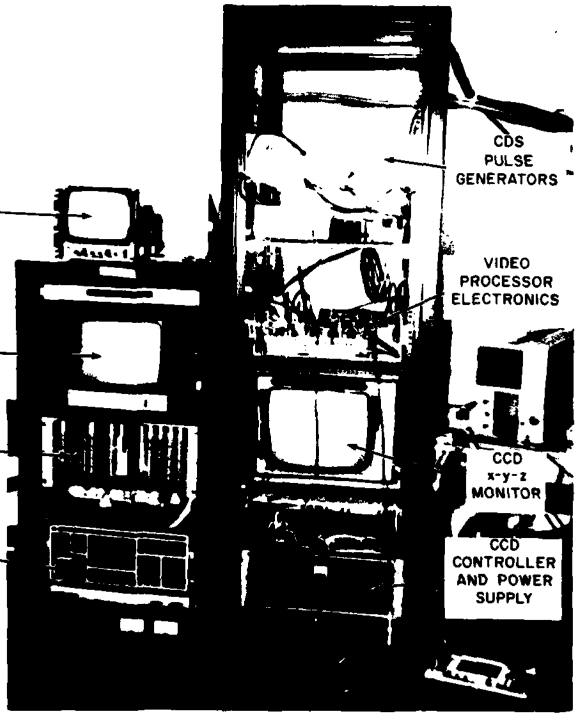

Fig. 12. CCD measurement system electronics.

A photograph of the CCD measurement system located in the base of the "B" telescope tower is shown in Fig. 12. Several of the subsystems are indicated in the figure.

III. DESCRIPTION OF TESTS

A. Brief Summary

The series of three tests covered in this report extended over a 14-month period. Each test was more extensive than the previous because of continuing improvements in the experimental electronics as well as increasing availability of CCD imager chips with improved characteristics.

For Test I, the CCD camera was operated only in the STARE mode. Observations were made and data gathered to evaluate predicted performance and the overall electro-optical signal path. In order to facilitate these measurements, a camera mount was fabricated which would interface with the telescope instrument rotator assembly and provide a chopper wheel shutter. Also, a liquid nitrogen supply was developed which would transfer LN_2 through relatively flexible insulated copper tubing to the CCD camera while allowing the telescope to be moved at moderate rates and adequate angles.

The Test II site-test included the operation of the CCD imager in both STARE and IMC modes. The STARE mode was used to permit camera alignment and provide electro-optical signal path and sensitivity data with lower-noise video electronics under cooled CCD conditions. The IMC experiments were the initial tests of the optical, electrical, and mechanical alignment of the scanning image across the imager focal plane, with the photoelectron charge being clocked in the imager chip. For Test III, a camera mount was fabricated to interface with the telescope prime focus spider, providing a chopper wheel shutter and minimum aperture blockage. The CCD imager chips for this test featured higher small-signal transfer efficiency, and fewer blemishes than previous devices.

Both STARE and IMC modes were used in the third site-test. For both cases, the CCD was cooled permitting low-light-level measurements. Specific calibration stars and satellites were acquired and scanned, permitting the first operational evaluation of IMC mode sensitivity and optical path responsivity. A unique test was conducted using both the 31-in. ETS telescopes, one with an Ebsicon camera and the other with the CCD camera, which demonstrated the observation dynamics of the IMC mode during continuous scan.

B. Test Outlines

In addition to the many electro-optical measurements conducted, several mechanical and operational tests were also performed. Table III provides an outline of the activities for each of the three site-test periods.

IV. DATA ANALYSIS

This section presents the results of the three CCD imager site-tests. The results described below include only samples from each of the test areas outlined in Table III. Data were gathered for all test areas as well as many additional, secondary, operational, and setup tests which will not be covered in this report.

A. Point Target Image on CCD Focal Plane

For quantitative measurements on any electro-optical system in which the point target image or seeing disc-of-illuminance is not centered on and is less than or equal to the imager pixel size, a point-spread-function analysis of the actual illuminance distribution per pixel must be performed in order to account for all light energy from the calibration object being observed. During the CCD tests at the ETS, large variations in seeing characteristics were observed, depending on existing atmospheric conditions as well as the particular telescope optics being used. The 31-in. telescopes at the ETS during observations exhibited nominal "good" seeing discs, with 80 percent of point target illuminance distributed over a 3-$\widehat{sec}$-diam disc as observed visually and with photographic plates. Such "good" seeing conditions were rarely observed during the three CCD site-test periods. Figures 13(a) and (b) show several samples of measured light distributions across a selected portion of a row of CCD pixels as observed during the first test. The trace in Fig. 13(a) indicates a typical point target distribution. With a Cassegrainian focal-plane scale factor of 0.754 mil/$\widehat{sec}$, 90 percent of the energy falls within a 7.9-$\widehat{sec}$-diam seeing

TABLE III OUTLINE OF ACTIVITIES FOR EACH SITE-TEST
TEST I (10 to 20 January 1978)
General Test Conditions CCD camera on 31-in. telescopes, Cassegrainian position CCD chip cooled to approximately −50°C Optical shutter used for 0.1-sec integration tests Night-sky background during nights of low-light-level observation were $\simeq 22^{m}\widehat{sec}^{-2}$ Moderate video gain and sensitivity CCDs had low charge transfer efficiency A. STARE Mode Only 1. Observe calibration solar-type stars and measure amplitudes for various integration times (t = 0.1, 0.5, 1, 5, 10, 20) to verify the electro-optical path model and sensitivity predictions for a wide range of star visual magnitudes. 2. Observe multiple stars in the CCD field-of-view of magnitudes within the camera dynamic range to evaluate field metric registration. 3. Observe solar-type stars of various magnitudes and over a wide range of seeing conditions and measure amplitude pulse-shape distributions. 4. Observe geosynchronous satellites in track mode and sidereal drive to evaluate streak dynamics.
TEST II (11 to 16 December 1978)
General Test Conditions High video sensitivity and CCD charge transfer efficiency CCD camera on 31-in. telescope "A," prime focus position Night-sky background was relatively high, $\simeq$ 17 to $18^{m}\widehat{sec}^{-2}$ even for best night of test period A. STARE Mode All low-light-level observations were made with the CCD chip cooled to approximately −10°C

TABLE III (Continued)
1. Observe solar-type calibration stars of various magnitudes and measure amplitudes for integration times of t = 0.1, 0.25 sec to verify electro-optical path model and sensitivity predictions. 2. For above observations, measure amplitude pulse-shape distributions for various seeing conditions. 3. Observe low-level calibration stars to provide signal sources for digitizer data recording program development. B. IMC Mode All observations were made with CCD chip at ambient temperature, $\simeq$+10° to 15°C Only positive declination scans were used No electronic lockup of telescope scan to CCD charge transfer was used The CCD focal plane was rotationally aligned to the telescope scan direction to within one resel, 2.9 $\widehat{\text{sec}}$, from the top pixel to the bottom pixel of the 100-pixel CCD imager columns The focal-plane scale factor resulted in a nominal telescope scan rate of 1104 $\widehat{\text{sec}}$/sec for a CCD transfer rate of 400 Hz or a total time delay integration time of 0.25 sec All video was scan converted to composite TV format and recorded on video-tape cassettes and with photographs of TV display monitors. 1. Scan at nominal 1104-$\widehat{\text{sec}}$/sec rate through star fields with appropriate magnitude objects and record imager fields-of-view to permit evaluation of point target smearing or distortion. 2. Scan at 10-percent greater-than-nominal rate to evaluate scan rate – charge transfer rate mismatch effects. 3. Scan at 10-percent lower-than-nominal rate to evaluate scan rate – charge transfer rate mismatch effects.
TEST III (26 March to 2 April 1979)
General Test Conditions CCD camera on 31-in. telescope "B," prime focus position CCD imager chip cooled to $\simeq$−40°C Periods of low night-sky-background ($\simeq 22^{m}\widehat{\text{sec}}^{-2}$) were available

TABLE III (Continued)

Light haze overcast present most of observation time

Several CCD imagers operated

Extensive effort to reduce electronic interference

A. STARE Mode

1. Observe solar-type calibration stars over a wide range of magnitudes at integration times from 0.1 to 0.9 sec to establish maximum sensitivity and responsivity operating points.
2. Measure amplitude pulse-shape distributions during above observations to evaluate existing seeing conditions.
3. Observe calibration stars, satellites, and star clusters to be recorded by the 32- × 32-sample digitizer system for two-dimensional pulse-shape analysis.

B. IMC Mode

A digital scan converter was used to provide expanded field-of-view in IMC mode increased to 480 × 384 pixels. The video was tape recorded and video monitors were photographed

CCD focal plane was rotationally aligned with telescope scan to better than 0.5 pixel

Only positive declination scans were used and at 1104-sec/sec scan rate

No lockup of the CCD transfer rate to the telescope scan encoder was needed or used

1. Low-light-level calibration stars were scanned and recorded for evaluation of IMC mode sensitivity and responsivity using an operator-activated frame capture in the digital scan converter.
2. Selected satellites were scanned and recorded.
3. Video level offsets and gain were adjusted from test-to-test to optimize sensitivity.
4. A scan was conducted synchronized with the other 31-in. telescope with an Ebsicon camera, and both CCD and TV videos were recorded for scan comparison.
5. Many scans were conducted to find sectors which were least degraded by telescope mount jitter.

disc. For very brief and rare occasions, the seeing improved to the extent shown in **Fig. 13(b)**, which at 3.2 $\widehat{sec}$ approaches the site seeing limit.

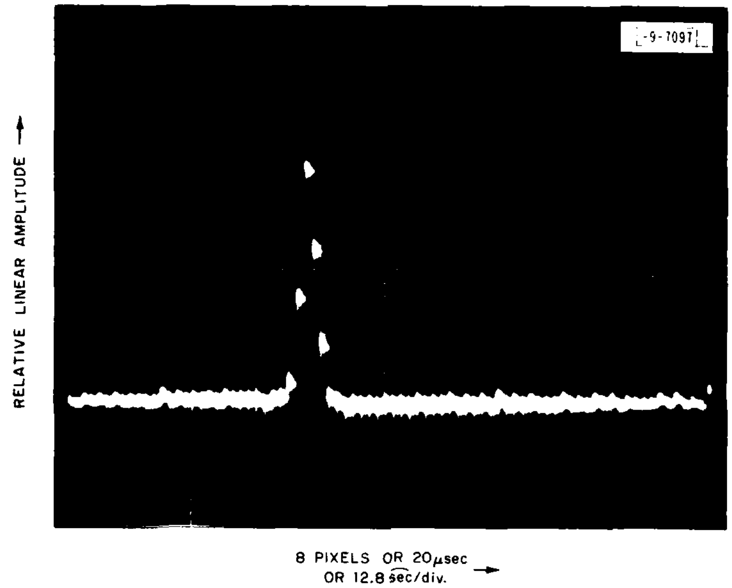

Fig. 13(a). Amplitude vs pixel for typical seeing condition of 5 pixels or 7.9 $\widehat{sec}$.

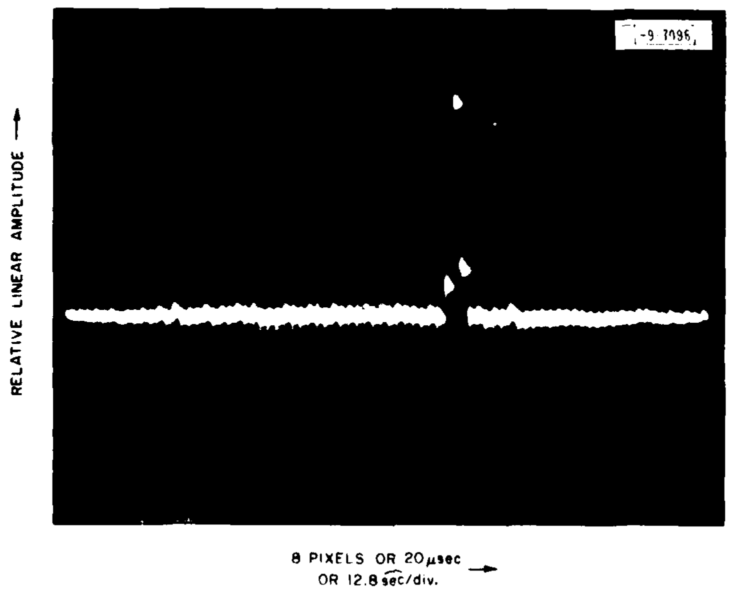

Fig. 13(b). Amplitude vs pixel for best seeing condition of 3.2 $\widehat{sec}$.

Amplitude measurements were made with the CCD imagers by photographing oscilloscope A-scope displays as in Figs. 13(a) and (b) with calibrated voltage scale for each calibrated object observed in the STARE mode. A Gaussian distribution curve was fitted to the A-scope traces, and values for σ_1 and peak voltage were obtained. It was assumed that the illuminance pixel distribution [point spread function (PSF)] was circularly symmetric two-dimensional Gaussian. Having the two-dimensional σ_2 and peak voltage V_p, the total voltage equivalent to all light falling on one pixel could be calculated from

$$V_T = V_p 2\pi\sigma_2^2 \tag{1}$$

where

$$\sigma_2 = 1.51\sigma_1 \quad . \tag{2}$$

This PSF correction was generated for each amplitude measurement and used in responsivity and sensitivity calculations.

B. Electro-Optical Responsivity

1. Definitions

A fundamental evaluation of the CCD imager capability involved the measurement of overall sensor responsivity which is defined as camera output voltage as a function of the magnitude of calibrated stars observed. The measurement results were compared with a comprehensive model of the entire electro-optical path, including atmosphere, telescope optics, CCD, and video electronics, to evaluate the consistency of the model. Parameters for the CCD imager model were derived from laboratory bench tests.

The predicted electro-optical sensor response was calculated using the following relationships:

$$M_v = 15 - 2.5 \log \left(\frac{\phi_s}{4.55 \times 10^4}\right) \tag{3}$$

and

$$\phi_s = \frac{V_T}{R_o G_v} \left(\frac{1}{A_T t Q \ell_T}\right) \tag{4}$$

for which,

M_v = visual magnitude of observed object,

ϕ_s = object photon flux at face of telescope,

V_T = single pixel video output voltage [see Eq. (1)],

R_o = CCD output responsivity ($\approx$2 μV/electron),

G_v = video voltage gain,

A_T = telescope apparent aperture,

t = integration time,

Q = CCD quantum efficiency,

ℓ_T = optical path loss due to (a) camera window and (b) atmospheric extinction.

The reference photon flux value of 4.55×10^4 photons/m^2/sec is for a 15-M_V solar object at the face of the telescope at an altitude of 4 kft through one site-air-mass.

2. Measurement Description

For periods of relatively stable seeing conditions for all three site-tests, several solar-type calibration stars were observed and camera output voltages were measured for a wide range of visual magnitudes and several imager integration periods. Because it was necessary to record the existing light-per-pixel distribution using A-scope traces to permit derivation of the appropriate PSF correction factors, observations were made in STARE mode only.

3. Results

In Test I, a large number of calibration stars were observed under varying conditions. The accumulated amplitude data are shown in Fig. 14 which is a plot of the stellar visual magnitude vs CCD camera video output voltage. The dashed line in this figure represents a least-squares fit to the measured data. The solid line is the calculated responsivity characteristic using the model described above. Although the measurements were made at several different integration times, the plot is normalized to 0.1-sec integration and single-pixel seeing performance. The degree of scatter in the plotted data can be attributed to inaccuracies in estimating the PSF correction factor and atmospheric variations which are difficult to model.

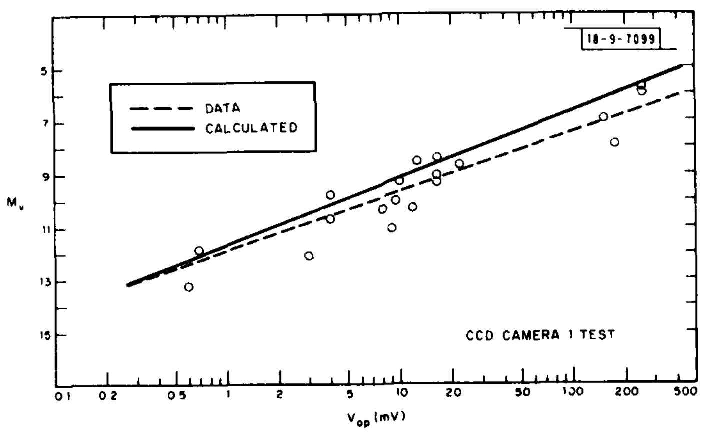

Fig. 14. Visual magnitude vs camera output.

Electro-optical responsivity measurements were conducted during all three site-tests using STARE mode and primarily solar-type calibration stars. Samples of the data compared with the design model are shown in Table IV. The samples were chosen to show the spread in agreement with model. Visual magnitudes from 9.3 to 13.9 M_V were used. This range of amplitudes gave sufficient signal-to-noise to eliminate the effects of noise from the measurements.

As seen in Table IV, surprisingly good agreement of better than 0.1 M_V was obtained between Test II measurements and model calculations. The model verification was not quite as impressive in Test III because of hazy sky conditions during this test period that could not be modeled sufficiently.

TABLE IV

CCD CAMERA ELECTRO-OPTICAL RESPONSE MODEL EVALUATION

	Object	M_v	PSF	Measured M_v	ΔM_v
Test I	SA-102-739	10.77	3.7	10.21	−0.56
	SA-100-607	10.06	3.1	9.32	−0.74
	SA-97-346	9.27	3.1	9.19	−0.08
	SA-99-90	10.24	3.8	9.41	−0.83
Test II	SA-115-350	11.05	1.8	11.02	−0.04
	I-69	12.27	2.0	12.32	+0.07
	SA-115-271	9.70	9.0	9.63	−0.07
	I-50	13.86	1.8	13.77	−0.09
Test III	SA-107-998	10.44	2.2	10.66	+0.22
	SA-107-691	11.08	2.1	11.45	+0.37
	SA-96-25	12.3	2.4	12.68	+0.38
	SA-96-517	11.43	3.5	11.10	−0.33

- Bright object used for high signal-to-noise
- Model validated to within 0.83 to 0.04 ΔM_v range

C. Electro-Optical Imager Sensitivity

1. Definitions

The evaluation of the CCD imager camera capability also included a measure of the observation sensitivity, which for these tests involved the comparison of the minimum-light-level stars visually detected on the CCD monitor with the calculated sensitivity limits based on the design model. The CCD camera sensitivity is not only limited by the electro-optical responsivity evaluated above, but also the CCD imager and video circuits electronic noise and existing night-sky background.

The predicted CCD camera sensitivity is calculated based on the approximate signal-to-noise relationship*

$$S/N \simeq \frac{\psi_{sig}}{(\psi_{sig} + \psi_{NSB} + N_I^2)^{1/2}} \qquad (5)$$

* R. Weber and T. H. Brooks, "The Limits of Detectability of a Low-Light-Level Point-Source Sensor as a Function of Telescope Aperture, Sensor Resolution, Night-Sky Background, and Pre-readout Electron Gain," Technical Note 1974-21, Lincoln Laboratory, M.I.T. (16 August 1974), DDC AD-785137/1.

where

ψ_{sig} = number of photoelectrons collected per pixel from the point target,

ψ_{NSB} = as above, but from night-sky background, and

N_i = rms number of noise electrons referred to the first video amplifier input at the specified CCD readout clock rate.

This relationship can be restated, solving for minimum target photon flux at the face of the telescope, with the resultant quadratic expression:

$$(Q^2 A_T^2 \ell_T^2 t^2)\phi_s^2 - A_T Q \ell_T t(S/N)^2 \phi_s - [\phi_B \alpha^2 A_T \ell_T Q t(S/N)^2 + N_i^2 (S/N)^2] = 0 \qquad (6)$$

where

ϕ_B = night-sky background photon flux,

α = resel angular size,

S/N = single-pixel signal-to-rms-noise ratio, assumed to be equal to 6 for automatic system detection,

and all other parameters are as defined in Eqs. (3) and (4) above.

After solving for the minimum photon flux, Eq. (3) above can be used to calculate the visual magnitude sensitivity limit.

Since the realistic seeing conditions cause some of the photon flux to be distributed over several pixels, the PSF correction as derived previously must be applied to the minimum photon flux calculated above, resulting in a degradation in sensitivity.

2. Measurement Description

Because the measured sensitivity limits for these electro-optical tests were essentially the minimum calibrated stars observed on the video monitors by the CCD camera operator rather than actual magnitude measurements, sensitivity tests were possible for both the STARE and IMC modes of operation. At several intervals during the low-light-level observations, the focus conditions were checked and updates on night-sky background and extinction were obtained when practicable.

In the STARE mode low-light-level observations, the calibration star field was observed after scan conversion on television monitors. The CCD readout frame rates were typically between 1 and 5 Hz. These continually updated video frames permitted a degree of observer "eye integration" on the TV monitor, thus requiring lower signal-to-noise ratios for detection. However, in the case of the IMC mode sensitivity tests, a single "onetime" video frame of the calibrated star field being scanned was captured, scanned, converted, and stored for viewing on the TV monitor. Observer "eye integration" was not possible and, therefore, signal-to-noise ratios of at least 3-to-6 were required for visual monitor detection in IMC mode.

Many of the low-light-level calibrated stars used in the tests were not directly observable with the Ebsicon 14-in. telescope sensor. Therefore, the CCD camera on the 31-in. telescopes was used to make the final target acquisitions for these sensitivity tests.

3. Results

A summary of the electro-optical sensitivity model evaluation results is presented in Table V for all three ETS site-tests. Shown are the integration times and differences in visual

TABLE V

CCD CAMERA ELECTRO-OPTICAL SENSITIVITY MODEL EVALUATION

	Integration Time (sec)	Calculated Sensitivity (M_v) (PSF corrected)	Minimum Object Observed (M_v)	Δ Sensitivity (M_v)
Test I	5.0	–	16.56	–
STARE	–	–	–	–
Test II	0.1	15.8	15.2	−0.6
STARE	0.25	16.6	16.0	−0.6
Test III	0.1	14.5	14.7	+0.2
STARE	0.9	16.9	17.2	+0.3
Test III	0.25	15.5	15.9	+0.4
IMC	–	–	–	–

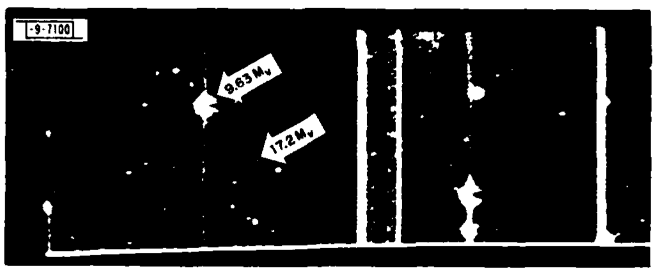

(a). Low video display threshold.

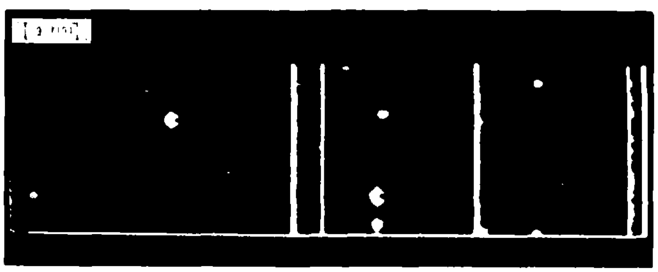

(b). Higher video display threshold.

Fig. 15(a-b). STARE mode low-light-level observations, Aquila field.

magnitude between predicted model sensitivity and the dimmer objects observed. The calculated sensitivity levels included values for existing night-sky background, and extinction, system electronic noise level, and PSF allowances for the indicated integration times and a S/N of 6.

Sensitivity predictions for Test I were not modeled because the CCD imagers that were available for this preliminary test had a fabrication defect which required relatively low clock voltages. The low clock voltages resulted in less-than-desirable array transfer efficiencies which limited low-light-level performance.

Although IMC mode operation was used in Test II, cooling of the CCD imager in IMC was not attempted and, therefore, low-light-level measurements for this mode were not considered.

The comparison results of Table V show excellent agreement with the model predictions. The plus signs in the results indicate observations at levels lower than the predicted limits. STARE mode amplitude measurements made on some of the minimum object observations showed signal-to-noise values greater than 6.

Examples of calibration star field observations are shown in the photographs in Figs. 15(a) through (d). Both STARE and IMC mode data are shown from the third site-test. The CCD video was scan-converted to TV format for display. The STARE mode fields [Figs. 15(a) and (b)] are 100 pixels high by 400 pixels wide. This field in Aquila (19:59.3 RA1950, +04°50' DEC 1950) shows a bright object 9.63 M_v and a nearby dim object 17.2 M_v, as indicated in Fig. 15(a). The circular blooming of the bright objects does not occur in the CCD imager, but is caused by point saturation blooming in the TV monitor. The charge spillover in the CCD remains in-column as seen in the figure. Blemishes in the CCD are displayed as columns and hot spots in the STARE mode.

For the IMC mode blemishes are displayed as bright columns only, as seen in Figs. 15(c) and (d) for which the field covers approximately 480 by 384 pixels made possible by the expand memory of the digital scan converter. The expanded stored field is a captured segment of the sky which was being continuously scanned by the telescope in declination at +1104 $\widehat{\text{sec}}$/sec with a constant RA value and sidereal drive running. Although the SA-100 star field for this field-of-view is only calibrated down to 13.9 M_v, interpolation of data from video tape recordings shows an observation of a star at 16 M_v with S/N > 6 as indicated in Fig. 15(c).

D. Satellite Observations

The series of preliminary site-tests covered in this report was mainly concerned with electro-optical measurements. No automatic satellite detection capability was tested. However, satellite objects were observed during the tests for functional qualitative demonstrations. More than twenty satellites were acquired and tracked in the STARE and IMC modes.

Figures 16(a) and (b) are examples of STARE mode satellite observations in Site-Test I. Shown are photographs of TV monitor presentations of the 100- × 400-pixel imager CCD video after scan conversion. Integration of ~8 sec was performed on the CCD followed by 0.1-sec readout of the CCD array. Video gain was greatly reduced for this test to eliminate saturation of electronics. Figure 16(a) shows the relatively bright satellites (No. 8585, CTS-1, at ≃12.5 M_v) in track at the right of the field-of-view. The bright streak to the left is caused by a bright star being in the field-of-view while tracking the satellite. The bright vertical streaks and small point objects are CCD blemishes. In Fig. 16(b) the telescope is locked in sidereal drive, with

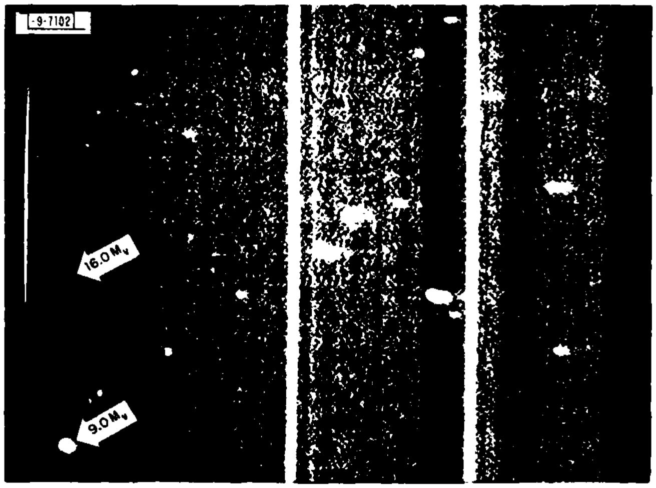

(c). Low video display threshold.

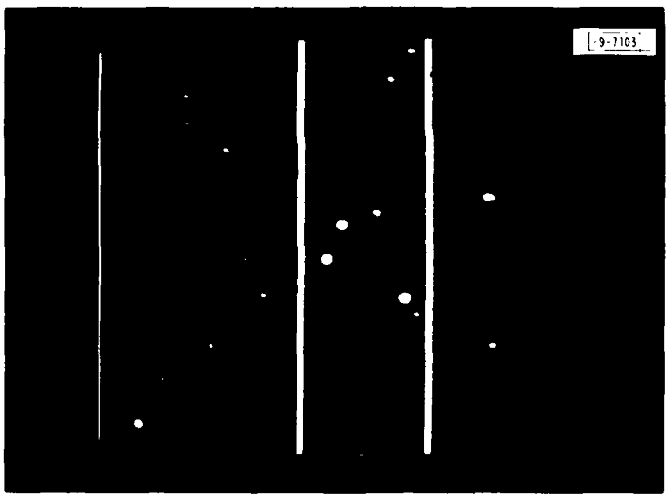

(d). Higher video display threshold.

Fig. 15(c-d). IMC mode low-light-level observations, SA-100 field.

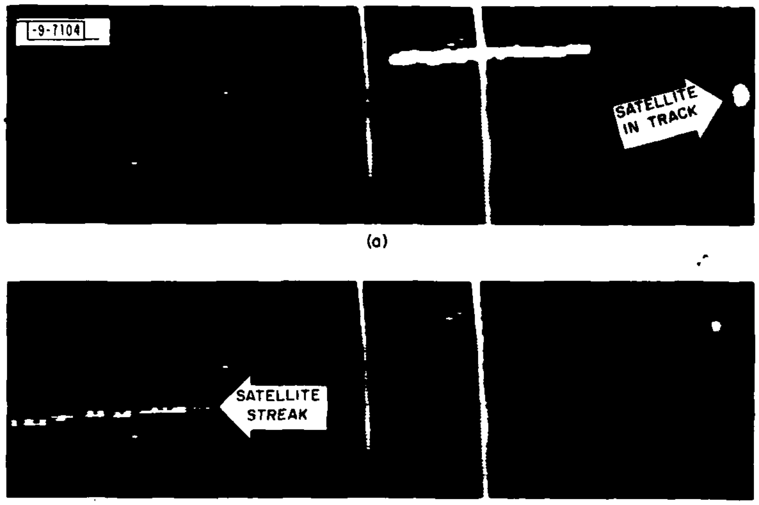

Fig. 16. Bright satellite observation and track: (a) satellite streak; (b) satellite in track.

a bright star in track at the right and the satellite forming a streak to the left of the field-of-view. The length of the streak is consistent with the integration period and the satellite rate of 15 $\widehat{\text{sec}}$/sec.

Typical satellite observations in IMC mode are shown in Figs. 17(a) and (b). For these tests, the scan rate gave an effective integration time of 0.25 sec. The telescope was scanning in declination at 1104 $\widehat{\text{sec}}$/sec with sidereal drive operating. No streak of the target satellite (No. 7318, ATS-6, 10.5 M_v) is indicated since dwell in pixel time was about equal to the integration time in column. Seeing conditions during the scan did not permit ultra low-light-level sensitivity; however, all point objects recorded are stars with CCD blemishes forming vertical bars. Much experience was gained in techniques for acquiring a satellite of interest with the IMC scans, which can be a problem with the limited field-of-view of the single-chip imager focal plane.

E. IMC Scan Alignment and Stability

One of the main objectives of these preliminary electro-optical site-tests was to determine the feasibility of stable IMC mode scans with the existing ETS telescopes, and to develop techniques to align the CCD imager in time and position with the scanning field image at the telescope focal plane.

In order to align the image scan within the CCD 100-pixel column, a bright object (star) was observed in STARE mode placed in the CCD field-of-view adjacent to a blemish column at the top of the field. The telescope was then scanned (in this case, in declination) slowly until the object was located at the bottom row. If the object had moved out-of-column, a slight rotation of the CCD camera mounted on the telescope was made and the test repeated until more than 50 percent of the point target seeing diameter stayed within the column.

For synchronizing the image motion scanned within a column to the CCD charge transfer rate of that column, two approaches were considered. The first approach was no form of lockup;

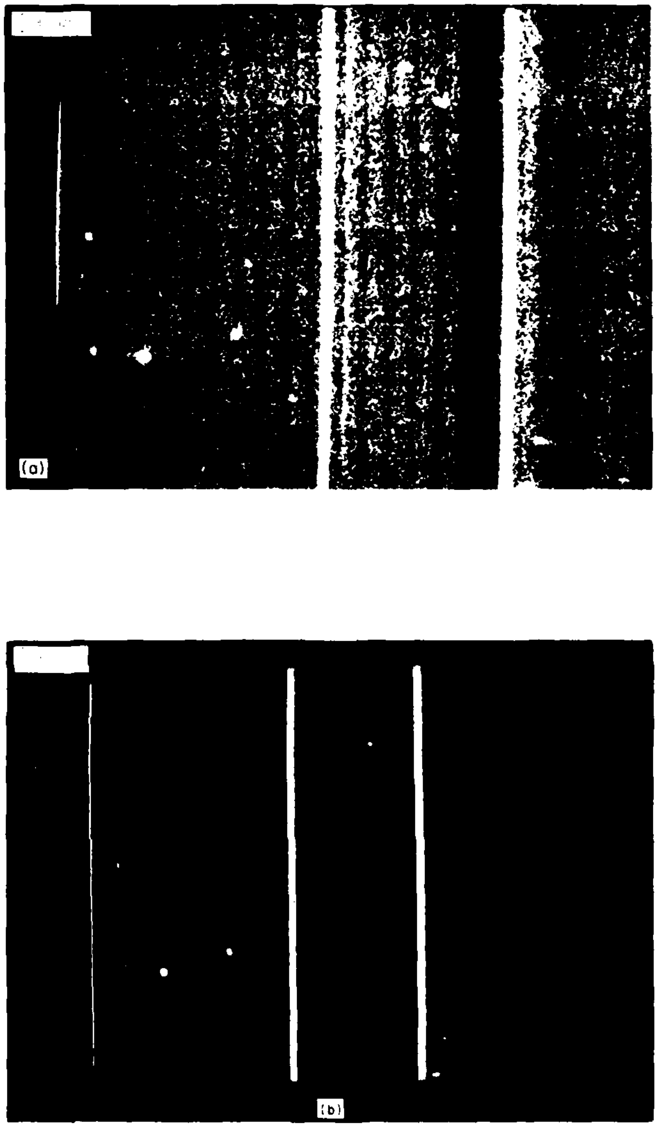

Fig. 17. Satellite ATS-6 acquired in IMC scan: (a) low video display threshold; (b) higher video display threshold.

the telescope scan rate was adjusted until charge transfer and image scan rates were equal. The second technique, using lockup, provided digital circuitry which measures (with selectable integration) the encoder output of the scanned axis of the telescope mount. The measured scan rate is used to determine the charge transfer clock rate of the CCD while the scan is proceeding. This lockup technique would not eliminate rate mismatch due to high frequency jitter, but would cancel slow rate drift mismatch.

The lockup technique could not be tested during the site-tests because anomalies in the telescope drive led to noisy encoder outputs. These anomalies have been removed since the last test period. Laboratory tests of the lockup circuitry indicate successful operation with simulated rate drift conditions.

During the IMC site-tests, telescope scan rate drift in joystick modes was found to be insignificant for the single-chip 0.25-sec scan periods; therefore, transfer rate lockup was not required. The photographs of video displays in Figs. 18(a) through (c) show the results of sync and non-sync IMC scans. The displays are captured frames of 100×400 pixels. In Fig. 18(a), the imaged stars are processed as circular objects indicating full synchronized scan. Seeing conditions were about 1.5 to 2.0 pixels for these tests, with low video gain and the CCD operating at ambient temperature. The telescope scan rate was intentionally increased by about 10 percent over the sync rate for Fig. 18(b), yielding an elongated image in the scan direction of about 10 out of 100 pixels, as would be expected. The slight slope deviation from vertical of the elongation is due to about one-half pixel misalignment of the CCD array with respect to the scan direction. A rate change of about 12-percent reduction was used for Fig. 18(c), resulting in the expected image smear or elongation of $\approx$13 to 14 pixels and with the opposite slope to vertical compared with the rate increase mismatch of Fig. 18(b).

The IMC scan tests indicate that for the 100-pixel (single-chip) scan case and in the absence of high-frequency mechanical jitter, the ETS telescope mounts are adequate for this mode of operation. For the future 5-chip focal-plane IMC site-tests, a scan rate stability with jitter and rate drift less than 0.1 percent is required over the 3-sec focal-plane scan period. The microprocessor-controlled telescope drives at ETS presently hold the scan rate to better than 0.1 percent, and photographic plate measurements indicate that the rate jitter should also be less than the required upper limit.

F. *Scan Comparison Demonstration*

During Site-Test III, a test was conducted which provided a demonstration of the operating dynamics of the CCD scanning in IMC mode compared with a STEP-STARE mode sensor such as the Ebsicon. The test involved the two 31-in. telescopes at the ETS simultaneously scanning in declination with sidereal drive at about the same right-ascension position.

Both telescopes scanned in positive declination at 1104 $\widehat{\text{sec}}$/sec. On one telescope, the CCD single-chip camera was mounted at the prime focus position yielding a field-of-view of about 0.3°. On the other telescope, the Ebsicon camera was mounted at the Cassegrainian position and operated in zoom, yielding a comparable field-of-view of about 0.5°.

The CCD camera video was scan-converted to TV format and sequential frames were digitally captured, displayed, and video-tape recorded. The Ebsicon camera video was also video-tape recorded. The two video-tape recordings were used to generate a movie strip of the simultaneous scans displayed side-by-side. Figure 19 shows a sample frame of the movie strip. The CCD video shows the utility of image motion compensation to generate useful video information

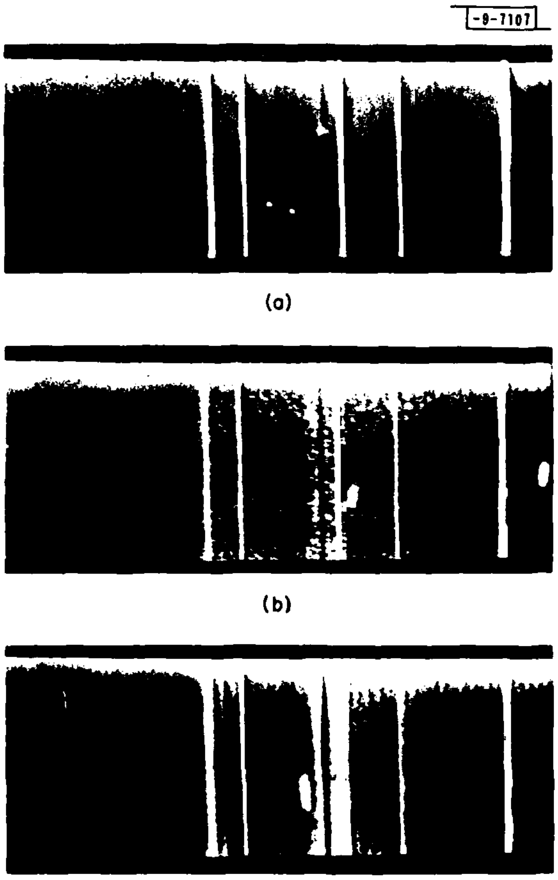

(a)

(b)

(c)

Fig. 18. IMC mode scan synchronization tests: (a) IMC scan full sync; (b) +10-percent scan rate offset; (c) −12-percent scan rate offset.

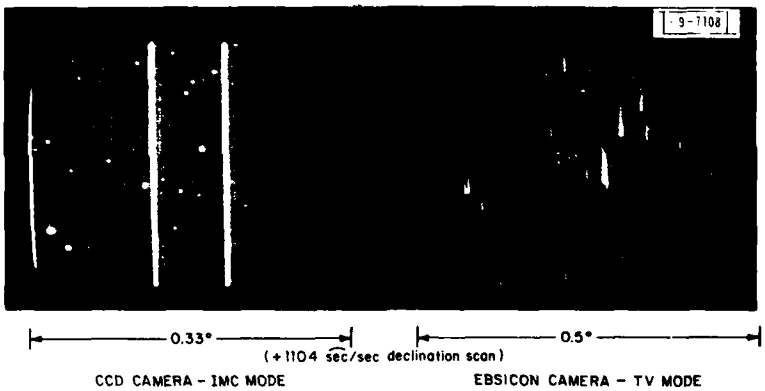

Fig. 19. Frame from movie of declination scan comparison of CCD and Ebsicon cameras.

during the efficient, continuous high-rate scan. The Ebsicon video display in the movie shows the high density of objects (stars) and the short-period time available in the high-rate scan for measurement.

V. CONCLUSIONS

These preliminary electro-optical field-tests of the Lincoln Laboratory-developed CCD imagers have achieved all test objectives and form a useful basis of experience for the future CCD automatic detection system tests at the ETS. Several factors encountered during the tests, which will have to be addressed for the next series of tests, are:

(a) The three site-tests provided many opportunities for measurement and evaluation of the realistic optical seeing conditions to be expected at the ETS. Although the "nominal-good" seeing provides approximately single-pixel imaging for the existing CCD design, the occurrence of this condition is very rare. Therefore, both an estimate of automatic detection system performance degradation as a function of seeing conditions as well as real-time video processing techniques for minimizing the effects of multi-pixel seeing are recommended for future tests.

(b) A considerable amount of electronic interference pickup in the low-noise video subsystems was encountered in these preliminary tests at the ETS which did limit the sensitivity performance compared with measurements conducted in the laboratory. Efforts will be required to locate and eliminate the sources of this interference.

(c) The dynamics of the telescope mounts at the ETS result in high frequency jitter as well as low frequency rate drift during the high rate scans for the IMC mode. Various components of the mount drives including torque motors and gear surfaces must be in top working condition to reduce these effects to acceptable levels. For each telescope mount there are particular regions of RA and DEC within which the most stable scans exist. The IMC mode testing should emphasize these regions.

(d) The operational and object acquisition techniques developed during these tests indicate that it is desirable to have the capability for fast switching between STARE and IMC modes of operation. This capability will permit real-time local metric calibration of the CCD field-of-view immediately preceding an IMC limited scan of a required target.

ACKNOWLEDGMENTS

The CCD imagers used in the reported tests were developed and characterized by Dr. Barry E. Burke of the Microelectronics Group. His expertise in solid-state device research as well as his interest and thoroughness in this program are greatly appreciated.

The authors also express their appreciation for the high-quality technician support provided by Kenneth M. Tibbets in fabrication and field-testing of the experimental system. The thorough preparations, expert support, and interest contributed by site personnel, particularly Dr. William E. Krag, Dr. Eugene W. Rork, David E. Beatty, Frank W. Thomason, and Robert L. Irelan, are greatly appreciated. The authors are also grateful to Marie Grey for her patience and expertise in typing this report, and to Edward Freedman for programming support for the STARE mode digitizer tests. The assistance of Anthony J. Yakutis in supplying video display, recording, and his experienced help in post-test data review are greatly appreciated.

UNCLASSIFIED

SECURITY CLASSIFICATION OF THIS PAGE (*When Data Entered*)

19) REPORT DOCUMENTATION PAGE		READ INSTRUCTIONS BEFORE COMPLETING FORM
1. REPORT NUMBER 18) ESD-TR-79-326	2. GOVT ACCESSION NO. AD-A088 270	3. RECIPIENT'S CATALOG NUMBER
4. TITLE (*and Subtitle*) Electro-Optical Tests of CCD Imagers at the GEODSS ETS		5. TYPE OF REPORT & PERIOD COVERED 9) Technical Report
		6. ~~PERFORMING ORG. REPORT NUMBER~~ Technical Report 539
7. AUTHOR(s) 10) Daniel F. Kostishack, Carl H. Gylfphe, Jr., Malcolm J. MacDonald, Norman G.S. Pong		8. ~~CONTRACT OR GRANT NUMBER(s)~~ 15) F19628-80-C-0002
9. PERFORMING ORGANIZATION NAME AND ADDRESS Lincoln Laboratory, M.I.T. P.O. Box 73 Lexington, MA 02173 16) 3221		10. ~~PROGRAM ELEMENT, PROJECT, TASK AREA & WORK UNIT NUMBERS~~ Program Element Nos.63428F and 12424F Project No.3221
11. CONTROLLING OFFICE NAME AND ADDRESS Air Force Systems Command, USAF Andrews AFB Washington, DC 20331 11) 20 Feb 80		12. REPORT DATE 20 February 1980
		~~13.~~ NUMBER OF PAGES 12) 36
14. MONITORING AGENCY NAME & ADDRESS (*if different from Controlling Office*) Electronic Systems Division Hanscom AFB Bedford, MA 01731 14) TR-539		~~15.~~ SECURITY CLASS. (*of this report*) Unclassified
		15a. DECLASSIFICATION DOWNGRADING SCHEDULE

16. DISTRIBUTION STATEMENT (*of this Report*)

Approved for public release; distribution unlimited.

17. DISTRIBUTION STATEMENT (*of the abstract entered in Block 20, if different from Report*)

18. SUPPLEMENTARY NOTES

None

19. KEY WORDS (*Continue on reverse side if necessary and identify by block number*)

- electro-optical devices
- charge-coupled device imagers
- STARE mode
- GEODSS
- deep space surveillance
- automatic detection system
- image-motion-compensation (IMC) mode

20. ABSTRACT (*Continue on reverse side if necessary and identify by block number*)

As part of the GEODSS-CCD Technology Program, a series of three electro-optical tests of CCD imagers was conducted on the GEODSS Experimental Test System (ETS) at Socorro, New Mexico. The tests were preliminary to establish the basis for developing and testing an advanced CCD automatic detection system which would provide improved sensitivity and scan coverage rate for GEODSS applications. These preliminary tests resulted in the successful demonstration of STARE and image-motion-compensation (IMC) modes of operation, and provided a thorough evaluation and verification of present CCD system design models. Also, interesting electro-optical performance levels were demonstrated, compared with existing GEODSS system designs.

DD FORM 1473 1 JAN 73 EDITION OF 1 NOV 65 IS OBSOLETE

UNCLASSIFIED 207650

SECURITY CLASSIFICATION OF THIS PAGE (*When Data Entered*)